Effects of ionization timing for off-resonant population transfer by postionization excitation in $N_2{}^+$

Youyuan Zhang, Erik Lötstedt ⬤, and Kaoru Yamanouchi ⬤*

Department of Chemistry, School of Science, The University of Tokyo, 7-3-1 Hongo, Bunkyo-ku, Tokyo 113-0033, Japan

We investigate postionization population transfer processes among the three low-lying electronic states—$X\,{}^2\Sigma_g^+$, $A\,{}^2\Pi_u$, and $B\,{}^2\Sigma_u^+$—of $N_2{}^+$ created in an ultrashort-pulsed intense laser field using a sudden turn-on model by explicitly including the ionization timing effect throughout the entire laser pulse. By adopting the rovibronic model in which the electronic, vibrational, and rotational degrees of freedom of $N_2{}^+$ are included, we have revealed that the population inversion between the $X\,{}^2\Sigma_g^+(v=0)$ state and $B\,{}^2\Sigma_u^+(v=0)$ state can be realized in the specific rotational quantum number ranges in the R- and P branches when ionization occurs around the central peak of the temporal shape of the laser field intensity. Based on the quasistationary Floquet theory, we have examined the laser field intensity dependence of the final population in the upper Floquet state, corresponding to the $B\,{}^2\Sigma_u^+(v=0)$ state of $N_2{}^+$, and revealed that the population transfer can be interpreted by the ionization at the ionization timing of $t=0$ as long as the laser field intensity is less than 4×10^{14} W/cm^2, while the ionization processes occurring in the entire range of the laser pulse need to be taken into account when the field intensity becomes larger.

I. INTRODUCTION

Air lasing is a phenomenon including a lasing signal associated with the creation of the population inversion of molecular ions, which are generated when an intense laser pulse is focused in air [1–5]. Because of a variety of possible applications in remote sensing and detection of pollutant species in the atmosphere [6], air lasing has been an attractive research target in the past decades. The mechanism of air lasing at 391 nm [1,7–15] had been mysterious for a long period until several years ago. The superradiance occurring when a group of excited molecules interact with light collectively and coherently has been suggested as a possible mechanism [13,16–18]. On the other hand, it has been reported that air lasing can be interpreted by the population inversion achieved between the vibrational ground state of the electronically excited $B\,{}^2\Sigma_u^+$ state and the vibrational ground state of the electronic ground $X\,{}^2\Sigma_g^+$ state of $N_2{}^+$, created by the irradiation of an intense near-infrared (near-IR) laser pulse [1,2,9,11]. In 2015, Xu *et al.* [9] interpreted the creation of the population inversion by introducing a mechanism of a sudden turn-on pulse, by which a nonresonant near-IR laser field transfers a population efficiently to the $B\,{}^2\Sigma_u^+$ state of $N_2{}^+$ from the $X\,{}^2\Sigma_g^+$ state, assisted by the $A\,{}^2\Pi_u$–$X\,{}^2\Sigma_g^+$ transitions, which depletes further the population in the $X\,{}^2\Sigma_g^+$ state. The mechanism of the population transfer by the sudden turn-on pulse was theoretically confirmed for a two-level system [19] using quasistationary Floquet theory [20], and the population inversion between the $B\,{}^2\Sigma_u^+$ and $X\,{}^2\Sigma_g^+$ state of $N_2{}^+$ was also interpreted well by quasistationary Floquet theory in terms of the time-dependent population transfer

between the vibrational levels in the $B\,{}^2\Sigma_u^+$ state and those in the $X\,{}^2\Sigma_g^+$ state [21]. The involvement of the $A\,{}^2\Pi_u$–$X\,{}^2\Sigma_g^+$ transition was confirmed by the Fourier transform of the lasing signal at 391 nm [22], and the giant enhancement [23] of the lasing at 391 nm confirmed the three-state $A\,{}^2\Pi_u$–$X\,{}^2\Sigma_g^+$–$B\,{}^2\Sigma_u^+$ coupling model [22,23] of the $N_2{}^+$ lasing.

On the other hand, the role of rotational excitation in $N_2{}^+$ has also been investigated to understand the $N_2{}^+$ lasing at 391 nm by pump-probe measurements [22,24], and the coherent couplings between the rotational levels of the $B\,{}^2\Sigma_u^+$ state and those of the $X\,{}^2\Sigma_g^+$ state were identified by time-resolved spectroscopy [25]. Rotational excitation was also proposed as a possible mechanism for creating the population inversion between the $B\,{}^2\Sigma_u^+$ state and the $X\,{}^2\Sigma_g^+$ state [26,27], and was later interpreted theoretically [28]. A pump-probe experiment was conducted later to record the temporal variation of the lasing intensity at 391 nm, and the Fourier transform revealed not only the $X\,{}^2\Sigma_g^+$–$B\,{}^2\Sigma_u^+$ coupling and the $X\,{}^2\Sigma_g^+$–$A\,{}^2\Pi_u$ coupling but also the rotational excitation in $N_2{}^+$[22]. The temporal evolution of the $N_2{}^+$ lasing was reproduced well by a complete theoretical model [29] in which both the $A\,{}^2\Pi_u$ − $X\,{}^2\Sigma_g^+$ − $B\,{}^2\Sigma_u^+$ vibronic coupling in $N_2{}^+$ [11,21,30] and the rotational excitations are incorporated.

In our previous theoretical simulations of the population inversion between the $B\,{}^2\Sigma_u^+$ state and the $X\,{}^2\Sigma_g^+$ state of $N_2{}^+$, it was assumed that the ionization occurs at the maximum amplitude of the electric field within an ultrashort laser pulse at the ionization rate evaluated by the molecular Ammosov-Delone-Krainov (MO-ADK) theory [31] and that the final populations in the vibrational levels in the $B\,{}^2\Sigma_u^+$ state depend on the laser field strength at the moment when $N_2{}^+$ is created by the ionization, as confirmed by quasistationary Floquet theory [21]. However, considering that the ionization can proceed not only at the maximum amplitude of the laser electric field

*kaoru@chem.s.u-tokyo.ac.jp

but also at the vicinity of the local maximum of the electric field amplitude, it becomes necessary for more quantitative discussion to integrate the yield of the ionization occurring during the entire duration of the laser pulse even though their contributions are not dominant, as was examined by a density matrix approach in recent publications [32–34].

In the present study, in order to incorporate the effect of the ionization occurring within the entire pulse duration in our sudden turn-on model for N_2^+ lasing, we investigate the ionization timing dependence of the postionization population transfer among the three electronic states, $X\,^2\Sigma_g^+$, $A\,^2\Pi_u$, and $B\,^2\Sigma_u^+$, of N_2^+ in an ultrashort near-IR laser field by including both the vibrational and rotational degrees of freedom.

II. ROVIBRONIC MODEL OF ROTATING N_2^+ AND VIBRONIC MODEL OF ALIGNED N_2^+

A. Rovibronic model of rotating N_2^+

Using the model developed in Ref. [28], we can calculate the time-dependent population transfer processes in N_2^+ by including all the electronic, vibrational, and rotational degrees of freedom. Within this model, which we hereafter call the rovibronic model, the time-dependent Schrödinger equation for a diatomic molecular ion is given by

$$i\hbar\frac{\partial}{\partial t}\Psi(\mathbf{r}, t) = H(t)\Psi(\mathbf{r}, t),\tag{1}$$

using the Hamiltonian operator H and the time-dependent wave function $\Psi(\mathbf{r}, t)$, represented under Born-Oppenheimer approximation as

$$\Psi(\mathbf{r}, t) = \sum_\alpha \sum_v \sum_K \sum_{m=-K}^{K} c_{\alpha v K m}(t)\psi_{\alpha v K m}(\mathbf{r}),\tag{2}$$

where $\mathbf{r}$ is a vector whose magnitude and direction represent the internuclear distance of a diatomic molecule and the direction of the internuclear axis in the space-fixed Cartesian coordinate system. The squared modulus of an expansion coefficient $c_{\alpha v K m}(t)$, given by

$$P_{\alpha v K m} = |c_{\alpha v K m}(t)|^2,\tag{3}$$

represents the probability of finding the system in the rotational state specified by a set of quantum numbers (K, m) in the vth vibrational state in the electronic state α, where K is a quantum number of the total angular momentum excluding the spin angular momentum and m is the projection of the total angular momentum on the space-fixed z axis.

A field-free eigenfunction is obtained by solving the stationary Schrödinger equation using the finite difference method,

$$H_0\psi_{\alpha v K m}(\mathbf{r}) = \varepsilon_{\alpha v K m}\psi_{\alpha v K m}(\mathbf{r}),\tag{4}$$

where H_0 is given using the reduced mass m_μ by

$$H_0 = -\frac{\hbar^2}{2m_\mu}\frac{\partial^2}{\partial \mathbf{r}^2} + V_\alpha(\mathbf{r}),\tag{5}$$

and the eigenfunction $\psi_{\alpha v K m}(\mathbf{r})$ is given by

$$\psi_{\alpha v K m}(\mathbf{r}) = \Phi_{\alpha v}^{(K)}(r)\Phi_{Km}^\alpha(\theta, \phi),\tag{6}$$

where $\Phi_{\alpha v}^{(K)}(r)$ represents the vibronic (vibrational and electronic) basis function and $\Phi_{Km}^\alpha(\theta, \phi)$ represents the rotational basis function.

To obtain the vibronic basis functions, we need to solve the radial part of the stationary Schrödinger equation given by

$$\left[-\frac{\hbar^2}{2m_\mu}\frac{\partial^2}{\partial r^2} + V_\alpha(r) + \frac{K(K+1)-k^2}{2m_\mu r^2}\right]\Phi_{\alpha v}^{(K)}(r)$$
$$= \varepsilon_{\alpha v}^{(K)}\Phi_{\alpha v}^{(K)}(r),\tag{7}$$

where k is the projection of the electronic orbital angular momentum on the molecular axis.

For $V_\alpha(r)$, the potential curves of either the $X\,^2\Sigma_g^+$, $A\,^2\Pi_u$, or $B\,^2\Sigma_u^+$ state of N_2^+ having a form of a Morse potential given by

$$V_{\alpha'}(r) = T_{e\alpha'} + D_{e\alpha'}(e^{-\alpha_{\alpha'}(r-r_{e\alpha'})} - 1)^2,\tag{8}$$

with the parameters given by the NIST Chemistry Webbook [35] are adopted. Using the finite difference method, we obtain the vibronic basis $\{\Phi_{\alpha v}^{(K)}(r)\}$ and the eigenenergy $\{\varepsilon_{\alpha v}^{(K)}\}$ of the rovibrational level specified by a set of quantum numbers, (K, v).

On the other hand, the rotational wave basis functions $\Phi_{Km}^\alpha(\theta, \phi)$, hereafter denoted as $|K, m, k\rangle$, are defined as [36]

$$|K, m, k\rangle = \frac{1}{\sqrt{2}}\sqrt{(K+m)!(K-m)!(K+k)!(K-k)!(2K+1)} \times \sum_\sigma (-1)^\sigma \frac{[\cos(\theta/2)]^{2K+k-m-2\sigma}[-\sin(\theta/2)]^{m-k+2\sigma}}{\sigma!(K-m-\sigma)!(m-k+\sigma)!(K+k-\sigma)!}e^{im\phi},\tag{9}$$

where θ is the polar angle and ϕ is the azimuth angle in the space-fixed coordinate system, and k is the projection of electronic orbital angular momentum on the molecular axis connecting two nitrogen nuclei. These wave functions can also be expressed in terms of the Wigner D functions [37]. For the $X\,^2\Sigma_g^+$ and $B\,^2\Sigma_u^+$ states, the projection k is $k = 0$ and $|K, m, 0\rangle$ becomes a spherical harmonic function.

For N_2^+, the rotational basis function $|K, m\rangle^\alpha$ is defined as

$$|K, m\rangle^\alpha = \begin{cases} |K, m, 0\rangle & \text{when } \alpha = X \text{ or } B, \\ (|K, m, 1\rangle + |K, m, -1\rangle)/\sqrt{2} & \text{when } \alpha = A_+, \\ (|K, m, 1\rangle - |K, m, -1\rangle)/\sqrt{2} & \text{when } \alpha = A_-. \end{cases}\tag{10}$$

It should be noted that for the doubly degenerate $A\,^2\Pi_u$ state, having $k = \pm 1$, the two basis functions, $|K, m\rangle^{A_+}$ and $|K, m\rangle^{A_-}$, are symmetric with respect to the transformation of $\theta \to \pi - \theta$, while the rotational basis functions, $|K, m, +1\rangle$ and $|K, m, -1\rangle$, are not symmetric with respect to the transformation of $\theta \to \pi - \theta$.

B. Solving time-dependent Schrödinger Equation for a diatomic molecular ion in rovibronic model

Inserting the complete rovibronic basis of Eq. (6) into the time-dependent Schrödinger equation, Eq. (1), and multiplying $\psi^*_{\beta v'K'm'}(\mathbf{r})$, representing the basis function of the electronic state β, from left and integrating over $\mathbf{r}$, we obtain

$$i\hbar \frac{d}{dt} c_{\beta v'K'm'}(t) = \sum_{\alpha=X,A_+,A_-,B} \sum_{v=0}^{v_{\max}} \sum_{K=0}^{K_{\max}}$$
$$\times \sum_{m=-K}^{K} c_{\alpha vKm}(t) H_{\beta v'K'm'\alpha vKm}(t), \quad (11)$$

where

$$H_{\beta v'K'm'\alpha vKm}(t) = \int_0^\infty \int_0^\pi \int_0^{2\pi} \psi^*_{\beta v'K'm'}(\mathbf{r}) H(t)$$
$$\times \psi_{\alpha vKm}(\mathbf{r}) dr \sin\theta d\theta d\phi. \quad (12)$$

In an intense laser field, the total Hamiltonian H of the system interacting with the laser field is written as

$$H(t) = -\frac{\hbar^2}{2m_\mu}\nabla^2 + V_\alpha + H_1(t) = H_0 + H_1(t), \quad (13)$$

where m_μ is the reduced mass of N_2^+, V_α is the interatomic potential energy of the electronic state α, and H_1 stands for the interaction with the laser field. Consequently, $H_{\beta v'K'm'\alpha vKm}(t)$ becomes

$$H_{\beta v'K'm'\alpha vKm}(t) = (H_0)_{\beta v'K'm'\alpha vKm} + (H_1)_{\beta v'K'm'\alpha vKm}(t), \quad (14)$$

where

$$(H_0)_{\beta v'K'm'\alpha vKm} = \langle \psi_{\beta v'K'm'} | H_0 | \psi_{\alpha vKm} \rangle$$
$$= \varepsilon_{\alpha vKm}\delta_{\alpha\beta}\delta_{v'v}\delta_{K'K}\delta_{m'm}, \quad (15)$$

and

$$(H_1)_{\beta v'K'm'\alpha vKm}(t)$$
$$= \langle \psi_{\beta v'K'm'} | H_1(t) | \psi_{\alpha vKm} \rangle$$
$$= \langle \psi_{\beta v'K'm'} | D_{\alpha\beta}(r) F_\theta^{\alpha\beta} \mathcal{E}(t) | \psi_{\alpha vKm} \rangle$$
$$= \langle \Phi_{\beta v'}^{(K')} | D_{\alpha\beta}(r) | \Phi_{\alpha v}^{(K)}(r) \rangle \langle \Phi_{K',m}^\beta | F_\theta^{\alpha\beta} | \Phi_{Km}^\alpha \rangle \mathcal{E}(t)$$
$$= p_{\alpha v\beta v'}^{(K'K)} p_{\alpha K\beta K'}^{(m)} \mathcal{E}(t). \quad (16)$$

In Eq. (15), $\varepsilon_{\alpha vKm}$ stands for the eigenenergy of the rotational state in the vth vibrational state of the electronic state α represented as $\psi_{\alpha vKm}$, $\mathcal{E}(t)$ in Eq. (16) stands for the amplitude

of the linearly polarized laser field at time t, and $F_\theta^{\alpha\beta}$ stands for the angular factor defined as

$$F_\theta^{\alpha\beta} = \cos(\theta)(\delta_{B\alpha}\delta_{X\beta} + \delta_{X\alpha}\delta_{B\beta}) + \frac{\sin(\theta)}{\sqrt{2}}(\delta_{A_\pm\alpha}\delta_{X\beta}$$
$$+ \delta_{X\alpha}\delta_{A_\pm\beta}), \quad (17)$$

which does not depend on the azimuth angle ϕ if the laser field is linearly polarized, so that the quantum number m is conserved during the interaction with the linearly polarized laser field. Therefore, $D_{\alpha\beta}F_\theta^{\alpha\beta}\mathcal{E}(t)$ in Eq. (16) represents the coupling between rovibronic states via the transition dipole moment $D_{\alpha\beta}$ between the two electronic states, α and β. As shown in the third line of Eq. (16), the coupling can be further decomposed into the vibrational coupling term,

$$p_{\alpha v\beta v'}^{(K'K)} = \langle \Phi_{\beta v'}^{(K')} | D_{\alpha\beta}(r) | \Phi_{\alpha v}^{(K)} \rangle, \quad (18)$$

and the rotational coupling term,

$$p_{\alpha K\beta K'}^{(m)} = \langle \Phi_{K',m}^\beta | F_\theta^{\alpha\beta} | \Phi_{Km}^\alpha \rangle. \quad (19)$$

The average probability of finding the system in the rotational state having the rotational quantum number K' in the vth vibrational state of the electronic state α is given by

$$\bar{P}_{\alpha vK'}(t) = \frac{1}{\zeta} \sum_{K''=0}^{K_{\max}} \sum_{m=-K''}^{K''} \left| c_{\alpha vK'm}^{X0K''m}(t) \right|^2 g_{K''} e^{\frac{-B_X K''(K''+1)}{k_B T_{abs}}}, \quad (20)$$

where $c_{\alpha vK'm}^{X0K''m}(t)$ are the coefficients determined as the solution of Eq. (1) under the initial conditions of $c_{\alpha vK'm}^{X0K''m}(t=0) = \delta_{X\alpha}\delta_{0v}\delta_{K'K''}$, B_X is the rotational constant of the $X\,^2\Sigma_g^+(v=0)$ state, k_B is the Boltzmann constant, T_{abs} is the absolute temperature, $g_{K''}$ is the nuclear spin statistical weight, which takes the values of $g_{K''} = 2$ for even K'' and $g_{K''} = 1$ for odd K'', and ζ is a normalization factor given by

$$\zeta = \sum_{K''=0}^{K_{\max}} g_K''(2K''+1) e^{\frac{-B_X K''(K''+1)}{k_B T_{abs}}}. \quad (21)$$

C. Vibronic model of aligned N_2^+

If we assume that N_2^+ is aligned in space and consider the population transfer dynamics in the linearly polarized laser field, the rotational motion can be neglected, so that the solution for Eq. (2) can be expressed as a linear combination of the electronic and vibrational states as

$$\Psi(\mathbf{r}, t) = \sum_{\alpha=X,A,B} \sum_{v=0}^N c_{\alpha,v}(t) \psi_{\alpha,v}(\mathbf{r}), \quad (22)$$

where the direction of $\mathbf{r}$ here is fixed at the alignment angle θ, defined as the angle between the molecular axis and the laser polarization direction.

The field-free basis set $\{\psi_{\alpha,v}\}$ is orthonormal and the wave function is normalized so that

$$\int_0^\infty |\Psi(r, t)|^2 dr = \sum_{\alpha=X,A,B} \sum_{v=0}^N |c_{\alpha,v}(t)|^2 = 1, \quad (23)$$

where $|c_{\alpha,v}(t)|^2$ represents the population of the vth vibrational state in the electronic state α, representing the probability of finding the system in the (α, v) state.

By adopting the same method introduced in Sec. II A, the vibrational basis can be calculated using the Schrödinger equation with a modified Hamiltonian given by

$$\left[-\frac{\hbar^2}{2m_\mu} \frac{\partial^2}{\partial r^2} + V_\alpha(r) \right] \Phi_{\alpha v}^{(K)}(r) = \varepsilon_{\alpha v}^{(K)} \Phi_{\alpha v}^{(K)}(r). \tag{24}$$

To perform simulations for N_2^+ with different orientation, the final populations calculated at all the possible alignment angles are summed up as an integral form of

$$P_{\text{final}} = \frac{1}{2} \int_0^\pi P(\theta) \sin(\theta) d\theta, \tag{25}$$

where $P(\theta)$ stands for the final population obtained at the alignment angle θ.

III. IONIZATION TIMING WITHIN A LASER PULSE

In our previous studies [9,19,21,28], we assumed that the ionization of N_2 proceeds at the maximum amplitude of the linearly polarized laser electric field within an ultrafast short laser pulse given by

$$\mathcal{E}(t) = \mathcal{E}^{\text{peak}} f(t) \cos(\omega t), \tag{26}$$

where ω is the frequency of the laser pulse and $f(t)$ represents a half-Gaussian envelope function, representing the sudden turn-on pulse, defined as

$$f(t) = \begin{cases} e^{-t^2/2\sigma_0^2} & (t \geqslant 0), \\ 0 & (t < 0). \end{cases} \tag{27}$$

To simulate the population transfer process induced by the ionization occurring at arbitrary time t_{ion} within the laser pulse duration, we modify the envelope function as

$$f(t) = \begin{cases} e^{-t^2/2\sigma_0^2} & (t \geqslant t_{\text{ion}}), \\ 0 & (t < t_{\text{ion}}), \end{cases} \tag{28}$$

where t_{ion} stands for the ionization timing within the laser pulse.

The ionization rate at the ionization timing t during an ultrashort laser pulse can be calculated by the molecular Ammosov-Delone-Krainov (MO-ADK) theory [31]. Because the laser field intensity ($\sim 10^{14}$ W/cm^2) reaches the barrier-suppression regime beyond the assumption required by the ADK theory, we employ the empirical equation [38] given by

$$W_{\text{emp}}(\mathcal{E}) = W_{\text{ADK}}(\mathcal{E}) e^{-\alpha(Z_c^2/I_p)(\mathcal{E}/\kappa^3)}, \tag{29}$$

where $\mathcal{E}$ is the field strength proportional to $\sqrt{I_0}$ ($\mathcal{E} \propto \sqrt{I_0}$), $W_{\text{ADK}}(\mathcal{E})$ is the MO-ADK ionization rate, $Z_c (= 1)$ is an effective charge for an active electron located at the asymptotically long distance from the ion core, $I_p = 0.573$ a.u. (15.6 eV) is the ionization potential of N_2, and $\alpha = 9.0$ is an empirical parameter introduced by the single-active electron (SAE) approximation taken from Ar atom as a substitute of N_2, and $\kappa = \sqrt{2I_p}$.

The time-dependent Schrödinger equation is solved with a sufficiently small time step to derive the time-dependent population dynamics. In the calculation, the wavelength of the sudden turn-on laser field given by Eq. (27) and Eq. (28) is set to be 800 nm and its duration is set to be 7 fs [full width at half maximum (FWHM)]. As the potential energy curves

of the three lowest-energy electronic states of N_2^+, that is, the $X\,^2\Sigma_g^+$ state, the doubly degenerate $A\,^2\Pi_u$ state (called the A_+ state and the A_- state), and the $B\,^2\Sigma_u^+$ state [28], the Morse potentials given in Ref. [35] are adopted and the coupling strengths among the rovibronic states are calculated using the transition dipole moments for the $B\,^2\Sigma_u^+ - X\,^2\Sigma_g^+$ and $A\,^2\Pi_u - X\,^2\Sigma_g^+$ transitions of N_2^+ given by Refs. [39,40]. The initial state at $t = 0$ is assumed to be the ground vibrational state in the $X\,^2\Sigma_g^+$ state of N_2^+ in a similar manner as in Ref. [29].

The following three different models for quantum levels involved in the population transfer are adopted. In all three models, the ionization timing dependence is investigated with sudden turn-on laser pulses whose initial ionization timing t_{ion} is in the range of $-2T \leqslant t_{\text{ion}} \leqslant 2T$, where $T = 2\pi/\omega$ is the period of the laser oscillation.

A. Rovibronic model

The time-dependent Schrödinger equation is solved with time step $\delta t = 1$ a.u., which is chosen so that the convergence of the populations in the respective vibrational states, obtained as the sum of the populations in the rotational levels, is reached below the level of 2.5×10^{-3} within a manageable computational cost to derive the time-dependent population dynamics in the three lowest-energy electronic states of N_2^+. In each electronic state, four vibrational states ($v = 0, 1, 2$, and 3) are included, and in each vibrational state, the highest rotational quantum number is set to be $K_{\text{max}} = 40$. The initial distribution in the rotational levels at $t = 0$ are given by the Boltzmann distribution at room temperature ($T_{\text{abs}} = 300$ K).

We do not include the effect of the rotational excitation of neutral N_2 in the calculation because we have previously shown [28] that rotational preexcitation before ionization changes the final populations in N_2^+ by an amount smaller than 0.01 for 28-fs laser pulses having an intensity of up to 6×10^{14} W/cm^2. In the present investigation, where we employ pulses having a duration of 7 fs, the effect of the rotational preexcitation is expected to be even smaller and can be neglected.

B. Vibronic model

The time step is set as $\delta t = 0.25$ a.u., which is taken so that the convergence of the populations in the respective vibrational states, obtained as the sum of the populations in the rotational levels, is reached below the level of 4.0×10^{-3} within a manageable computational cost, and the three lowest-energy electronic states of N_2^+, i.e., the $X\,^2\Sigma_g^+$, $A\,^2\Pi_u$, and $B\,^2\Sigma_u^+$ states, with their four lowest-energy vibrational states ($v = 0, 1, 2$, and 3) are included. The final populations transferred to the $B\,^2\Sigma_u^+(v = 0)$ state are obtained at the different alignment angle ($0 < \theta < \pi$) with the interval of $\delta\theta = 0.1$ rad, and are integrated over the entire laser pulse duration according to Eq. (25).

C. Two-level model

This simplest model can be regarded as a special case of the vibronic model in which the alignment angle is fixed at $\theta = 0$.
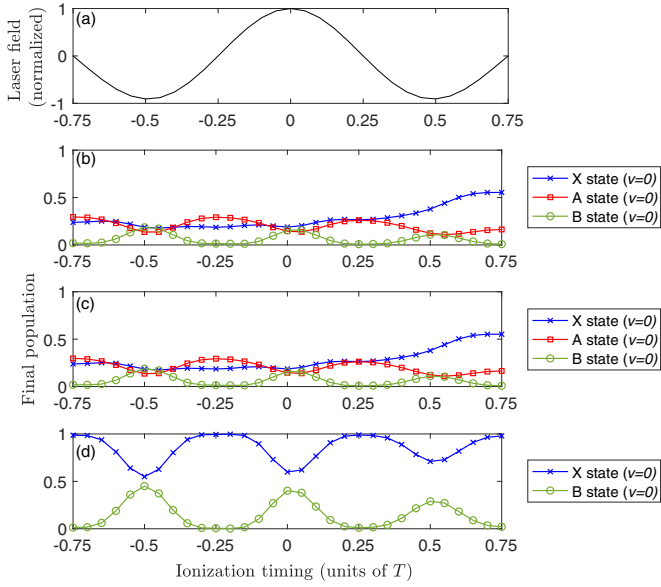
FIG. 1. (a) Illustration of the laser field $\mathcal{E}(t)$. (b) Final populations in the vibrational ground states of the $X^2\Sigma_g^+$, $A^2\Pi_u$, and $B^2\Sigma_u^+$ states of N_2^+ at different ionization timings with an interval of $T/20$ (~ 0.13 fs) calculated in the rovibronic model, including the four lowest vibrational states in each electronic state. (c) Final populations in the vibrational ground states of the $X^2\Sigma_g^+$, $A^2\Pi_u$, and $B^2\Sigma_u^+$ states of randomly aligned N_2^+ integrated over the alignment angle at the ionization timings. The four lowest vibrational states are included in the respective electronic states. (d) Final populations in the vibrational ground states of the $X^2\Sigma_g^+$ state and the vibrational ground state of the $B^2\Sigma_u^+$ state of N_2^+ aligned parallel to the laser polarization direction ($\theta = 0$) at the ionization timings. Only the two vibrational ground states are included so that it becomes a two-level system. In all panels, the laser field intensity is set to be 4×10^{14} W/cm^2.

When N_2^+ is aligned in space so that the N–N axis is parallel to the polarization direction of the laser field ($\theta = 0$), the $X^2\Sigma_g^+$ state can be coupled with the $B^2\Sigma_u^+$ state via the parallel dipole transition, but cannot be coupled with the $A^2\Pi_u$ state because the $A^2\Pi_u$–$X^2\Sigma_g^+$ transition is a perpendicular dipole transition. Therefore, in this aligned configuration, as long as we consider only the vibrational ground state of the $X^2\Sigma_g^+$ and the vibrational ground state of the $B^2\Sigma_u^+$ state, the system can be treated as a simple two-level model.

IV. RESULTS AND DISCUSSION

A. Comparison of three models

As can be seen in Fig. 1, the final populations in the vibrational ground states of the three electronic states obtained using the laser field intensity of 4×10^{14} W/cm^2 depend on the ionization timing within the laser pulse duration. In addition, as we demonstrated in Ref. [21], the final population in the $B^2\Sigma_u^+$ state depends sensitively on the field strength at which N_2 is ionized to N_2^+.

The result obtained by the rovibronic model, shown as Fig. 1(b), and that obtained by the vibronic model, shown in Fig. 1(c), are almost the same and show that the rovibronic
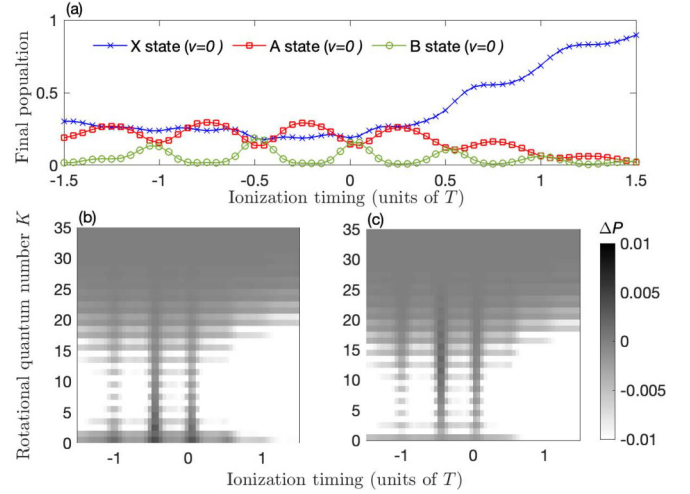

FIG. 2. (a) Final population in the vibrational ground states of the $X^2\Sigma_g^+$, $A^2\Pi_u$, and $B^2\Sigma_u^+$ states of N_2^+ obtained by the rovibronic model at different ionization timings, including the four lowest vibrational states in each electronic state. (b) Final population difference between the rovibronic levels for the R-branch transitions of the $B^2\Sigma_u^+(v=0)$–$X^2\Sigma_g^+(v=0)$ emission at different ionization timings, including four vibrational levels in each electronic state. (c) Final population difference between the rovibronic levels for the P-branch transitions of the $B^2\Sigma_u^+(v=0)$–$X^2\Sigma_g^+(v=0)$ emission at different ionization timings. Black indicates that population inversion is achieved, while white indicates that the population inversion is not achieved. In all the panels, the laser field intensity is set to be 4×10^{14} W/cm^2.

model and the vibronic model agree well with each other as long as the final populations in the vibrational levels are concerned. The rovibronic model needs to be adopted when we discuss the rotationally resolved lasing signals as in the case of the investigation of the P-branch and R-branch lasing emission lines [29].

As shown in Figs. 2(b) and 2(c), population inversion can be achieved between the specific rotational levels in the $B^2\Sigma_u^+$ and $X^2\Sigma_g^+$ states even when the total population in a vibrational state in the $B^2\Sigma_u^+$ state integrated over the rotational levels is not inverted with respect to the total population in a vibrational state in the $X^2\Sigma_g^+$ state integrated over the rotational levels, as was shown in our recent study [28]. As can be seen in Fig. 2(b), the R-branch emission can be realized between the low-lying rotational levels ($K < 10$) when the ionization occurs at around $t_{ion} = -2\pi/\omega, -\pi/\omega$ and 0, that is, $t_{ion} = -T, -T/2$, and 0, which are the peak regions of the optical cycles. On the other hand, as shown in Fig. 2(c), the P-branch emission can be realized between the highly excited rotational levels ($10 < K < 25$).

As shown in Fig. 2(a), the vibrational population difference between the $B^2\Sigma_u^+(v=0)$ and $X^2\Sigma_g^+(v=0)$ state varies depending on the ionization timing, but the inversion between the net populations is not achieved under the current laser field conditions. However, as shown in Fig. 2(b), the lasing emission becomes possible between the low rotational levels at the ionization timings of $t_{ion} = -2\pi/\omega, -\pi/\omega, 0$, that is, $t_{ion} = -T, -T/2$, and 0.
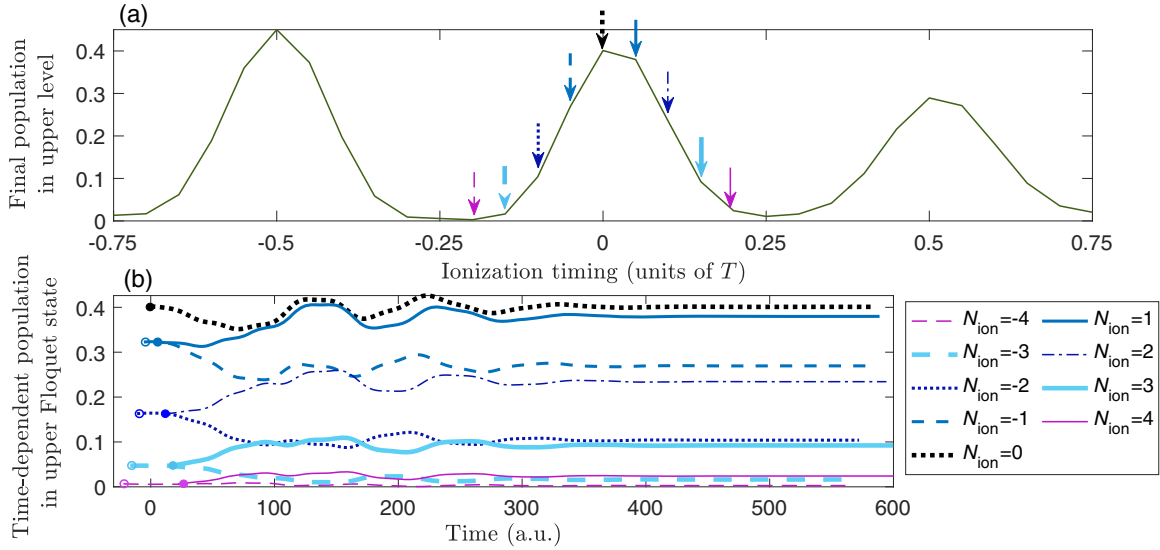
FIG. 3. (a) Final populations in the upper Floquet state of the two-level system as a function of the ionization timing. The downward arrows represent the ionization timings at $t_{ion} = N_{ion}\pi/10\omega = N_{ion}(T/20) = N_{ion} \times 5.54$ a.u. ($N_{ion} = -4, -3, -2, -1, 0, 1, 2, 3,$ and 4). The laser field intensity is 4×10^{14} W/cm^2. (b) Time-dependent populations in the upper Floquet state obtained at different ionization timings within the central optical cycle of the laser pulse.

According to the quasistationary Floquet theory employed in Ref. [21], the populations in the B $^2\Sigma_u^+$ state obtained at a particular ionization timing before the peak of the pulse ($t_{ion} = -t_0 < 0$) and an ionization timing after the pulse ($t_{ion} = t_0 > 0$) should be the same. However, as shown in Fig. 1, the final population in the B $^2\Sigma_u^+(v = 0)$ state obtained at $t_{ion} = t_0$ is slightly larger than that obtained at $t_{ion} = -t_0$ for $0 < t_0 \leqslant 3T/4$ in all three models. For example, ΔP defined as $P_{B0}(t_{ion} = +T/20) - P_{B0}(t_{ion} = -T/20)$ takes the values of 0.0610 for the rovibronic model, 0.0549 for the vibronic model, and 0.1303 for the two-level model. This slight asymmetry appearing even when the system is reduced to the simplest two-level system can be ascribed to the nonadiabatic effect induced by the ultrashort pulse employed in the present simulation as explained below for the two-level model using the Floquet formalism.

B. Population in upper Floquet level

Using the quasistationary Floquet formalism developed in Ref. [19], the two levels in the two-level model can be represented as two time-dependent Floquet states $|\Phi_q(t)\rangle(q = 1, 2)$, which are time-dependent Floquet basis states defined as

$$|\Phi_q(t)\rangle = \sum_{n=-\infty}^{\infty} \sum_{\alpha=1}^{2} \phi_{\alpha,q}^{(n)} |\alpha\rangle e^{-in\omega t}. \quad (30)$$

Thus, the wave function of the system can be expressed as the linear combination of these independent solutions,

$$|\Psi^{(Floquet)}(t)\rangle = \sum_{q=1}^{2} k_q e^{-i\varepsilon_q \omega t} |\Phi_q(t)\rangle, \quad (31)$$

where the coefficients k_q are constants in the quasistationary Floquet theory [19] as long as the temporal changes in the envelope of the laser pulse can be treated adiabatically. The

coupled differential equations for $\{k_q(t)\}$ can be given by [41]

$$\frac{dk_q(t)}{dt} = -\mathcal{E}_0 \frac{df(t)}{dt} \sum_{r=1}^{2} \left\langle \Psi_q^{\mathcal{E}_0 f(t)} \middle| \frac{\partial}{\partial \mathcal{E}_0} \Psi_r^{\mathcal{E}_0 f(t)} \right\rangle k_r(t), \quad (32)$$

where $\mathcal{E}_0$ represent the oscillation amplitude of the laser field. In the adiabatic limit, $df(t)/dt = 0$, and consequently, the coefficients $\{k_q(t)\}$ are constant in time.

However, in an intense and ultrashort laser field whose FWHM is as short as 7 fs, the nonadiabatic transitions governed by the matrix elements, $\langle\Psi_q^{\mathcal{E}_0 f(t)}|\partial\Psi_r^{\mathcal{E}_0 f(t)}/\partial\mathcal{E}_0\rangle$, as well as by $df(t)/dt$ cannot be neglected. This type of nonadiabatic transition is not included in the quasistationary Floquet formalism adopted here or in Refs. [19,21], where the Floquet states are obtained at t assuming a periodic field with the amplitude $\mathcal{E}_0 = \mathcal{E}^{peak}f(t)$. The nonadiabatic transitions can be incorporated straightforwardly in the quasistationary Floquet theory by propagating the Floquet states in time with the time-dependent coupling in a manner described in Ref. [20].

The dependence of the ionization timing on the population in the upper Floquet basis state is plotted in Fig. 3(b), which is obtained by the projection of the time-dependent wave function of N$_2^+$ onto the corresponding upper Floquet state. When the ionization occurs at the maximum amplitude of the laser field at $t_{ion} = 0$, the population in the upper Floquet state takes the largest value after the interaction with the laser field among the nine different ionization timings of $t_{ion} = N_{ion}T/20$, with $N_{ion} = -4, -3, \ldots, 4$. It is interesting to note that the population obtained for $t_{ion} = T/20$ is larger by 0.13 than that obtained for $t_{ion} = -T/20$, even though the ion yields, that is, the populations at the ionization timings, are the same. Similarly, the yield of the upper Floquet state for $t_{ion} = N_{ion}T/20$ is larger than that for $t_{ion} = -N_{ion}T/20$ when $N_{ion} = 2, 3, 4$. The larger efficiency of the population transfer to the upper Floquet state at the later ionization with respect to the central peak of the laser field than at the earlier ionization
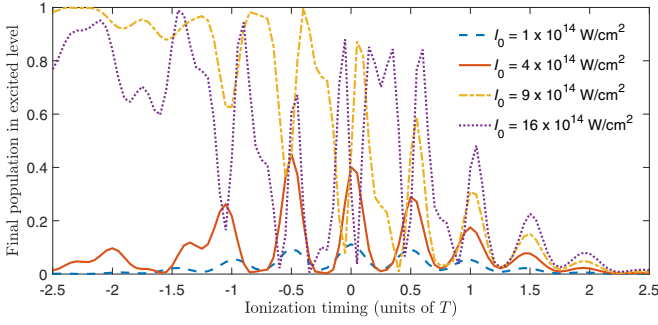
FIG. 4. Final populations in the excited level of the two-level system as a function of the ionization timing at the four different peak laser field intensities.

can be interpreted by the difference in the nonadiabatic effect in the course of the interaction with the laser field after the ionization.

C. Dependence of final populations on laser field intensity

1. Ionization dependence at different field strengths

We examine the effect of the ionization timing on the population transfer in the two-level model using the field-free basis in the wide range of the peak intensity of the laser field ($I_0 = 0$–16×10^{14} W/cm^2). The results of the simulation are shown in Fig. 4. At $I_0 = 1 \times 10^{14}$ W/cm^2 and $I_0 = 4 \times 10^{14}$ W/cm^2, the final population in the excited level follows the oscillation of the laser pulse, that is, the larger the light field intensity becomes at the moment of ionization, the more the population is transferred to the excited level. However, at $I_0 = 9 \times 10^{14}$ W/cm^2 and $I_0 = 16 \times 10^{14}$ W/cm^2, the population transfer tends to be more efficient in the earlier part of the laser pulse.

At the weak field intensities of 1×10^{14} W/cm^2, the final population in the upper level is more or less symmetric with respect to the central peak of the amplitude of the laser field, which is in good agreement with the result shown in Fig. 3(a) obtained by the quasistationary Floquet theory. However, as the laser field intensity becomes larger, this symmetry in the final population starts disappearing at $I_0 = 4 \times 10^{14}$ W/cm^2, and the final population in the excited level becomes larger at the later ionization timings ($t_{\mathrm{ion}} > 0$) than at the earlier ionization timings ($t_{\mathrm{ion}} < 0$) in the close vicinity ($-0.1 < t_{\mathrm{ion}}/T < 0.1$) of the center of the laser pulse. This type of behavior cannot be described by the quasistationary Floquet theory adopted here as well as in Refs. [19,21], because the nonadiabaticity represented by the matrix elements and $dk_q(t)/dt$ appearing on the right hand side of Eq. (32) cannot be neglected in the intense 7-fs laser field.

2. Final population given by three cases of ionization timing

In the simulation of the postionization population transfer processes, we examine three cases of ionization timing within the laser pulse. In all three cases, we adopt the two-level model composed of the X $^2\Sigma_g^+$ ($v = 0$) state and the B $^2\Sigma_u^+$ ($v = 0$) state of N$_2^+$, whose molecular axis is aligned along the laser polarization direction. In Case I, we assume that the ionization proceeds only at $t = 0$, that is, at the maximum amplitude of

the laser electric field in the same manner as in our previous studies [21,28,29]. The final population in the B $^2\Sigma_u^+$ ($v = 0$) state is defined as

$$P_{\mathrm{B0}}^{(\mathrm{I})} = P_{\mathrm{B0}}(t_{\mathrm{ion}} = 0), \tag{33}$$

where $P_{\mathrm{B0}}(t_{\mathrm{ion}} = 0)$ is the final population in the B $^2\Sigma_u^+$ ($v = 0$) state obtained assuming that the ionization occurs at $t_{\mathrm{ion}} = 0$.

In Case II, we assume that ionization proceeds at all the local maxima of the amplitude of the laser electric field within the laser pulse at $t_{\mathrm{ion}} = N_{\mathrm{ion}}\pi/\omega = N_{\mathrm{ion}}T/2$, and the final populations are obtained as the sum of the respective contributions from the different ionization timings with the weights proportional to the ionization rates,

$$P_{\mathrm{B0}}^{(\mathrm{II})} = B_{\mathrm{II}}^{-1} \sum_{N_{\mathrm{ion}}=-5}^{5} W_{\mathrm{emp}}[\mathcal{E}(N_{\mathrm{ion}}T/2)]P_{\mathrm{B0}}(t_{\mathrm{ion}} = N_{\mathrm{ion}}T/2), \tag{34}$$

where W_{emp} is the MO-ADK ionization rate defined in Eq. (29). In Eq. (34), a normalization factor, $B_{\mathrm{II}} = \sum_{N_{\mathrm{ion}}=-5}^{5} W_{\mathrm{emp}}[\mathcal{E}(N_{\mathrm{ion}}T/2)]$, is introduced so that the total ionization probability becomes normalized to be 1 regardless of the laser intensity employed in the simulation.

When the ionization probability becomes large so that most of the N$_2$ molecules are ionized before the peak of the pulse, we have to include the effect of the depletion of N$_2$ molecules when taking the sum over the ionization timings. The depletion of N$_2$ is accounted for by replacing $W_{\mathrm{emp}}(t)$ in Eq. (34) by a modified ionization rate $W_{\mathrm{emp}}'(t)$ defined as

$$W_{\mathrm{emp}}'(t) = W_{\mathrm{emp}}(t)e^{-\int_{-\infty}^{t} W_{\mathrm{emp}}(t')dt'}, \tag{35}$$

where the factor $e^{-\int_{-\infty}^{t} W_{\mathrm{emp}}(t')dt'}$ represents the time-dependent population of neutral N$_2$ molecules.

In Case III, by assuming that the ionization followed by the population transfer proceeds over the entire range of the laser pulse duration, we calculate the extent of the population transfer at equally spaced ionization timings with the spacing of $T/20$, including the ionization timing at the maximum amplitude in the center of the Gaussian pulse. The final population is obtained as the sum of the respective contributions with the weights proportional to the ionization rate,

$$P_{\mathrm{B0}}^{(\mathrm{III})} = B_{\mathrm{III}}^{-1} \sum_{N_{\mathrm{ion}}=-50}^{50} W_{\mathrm{emp}}[\mathcal{E}(N_{\mathrm{ion}}T/20)]P_{\mathrm{B0}}(t_{\mathrm{ion}} = N_{\mathrm{ion}}T/20), \tag{36}$$

with $B_{\mathrm{III}} = \sum_{N_{\mathrm{ion}}=-50}^{50} W_{\mathrm{emp}}[\mathcal{E}(N_{\mathrm{ion}}T/20)]$. Similarly to Case II, we consider the effect of the depletion of N$_2$ by the replacement of W_{emp} in Eq. (36) by W_{emp}' defined in Eq. (35).

In Cases II and III, similarly to previous investigations [32–34,42], we assume that final populations created at different ionization timings can be added incoherently. This assumption can be rationalized by the fact that no coherence is generated in the N$_2^+$ ion after the ionization because of the different parities of the electronic states [43]. In addition, within a short pulse, electrons emitted at different ionization timings have different final momenta so that contributions from different ionization timings are in principle distinguishable events.
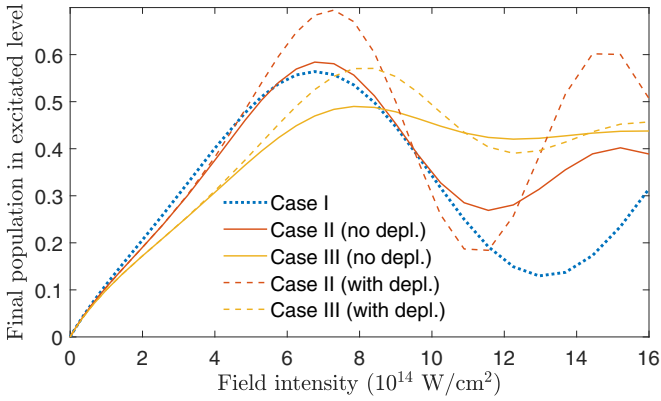
FIG. 5. Final populations in the excited level of the two-level system as a function of the peak laser field intensity using three different cases (Cases I–III) of the ionization timings within the temporal duration of the laser pulse. The final populations obtained with and without the depletion effect of N_2 are shown with broken lines and solid lines, respectively.

The final population in the upper level is calculated using the three different cases (Cases I–III) of the ionization timings within the temporal duration of the laser pulse in a wide range of laser field intensities. The results of the simulations are shown in Fig. 5.

When Case I is adopted for the choice of the ionization timings, in which only the ionization at the central peak of the temporal variation of the laser field intensity is considered, the final population in the upper level is overestimated by 15%–20% in the lower laser field intensity region than about $8 \times 10^{14} \, \text{W/cm}^2$ and is underestimated significantly in the intensity range of $8-16 \times 10^{14} \, \text{W/cm}^2$ compared with the results obtained when Case III is adopted, which is considered to give the most accurate estimate of the final populations within the present ionization model.

When Case II is adopted for the choice of the ionization timings, in which the ionization at the respective local maxima of the periodical variation of the laser field intensity is considered, the extent of the overestimation of the final population in the upper level in the lower-intensity range is slightly smaller than Case I and the extent of the underestimation in the high-intensity region is much smaller than Case I. When the intensity exceeds $10^{15} \, \text{W/cm}^2$, the final population in the upper level obtained with the N_2 depletion effect exhibits a significant difference from that obtained without the N_2 depletion effect.

Therefore, it can be said that as long as the laser field intensity range is lower than $4 \times 10^{14} \, \text{W/cm}^2$, Cases I and II are good choices of ionization timings for estimating quantitatively the final populations of the two levels even though the estimate can be underestimated to a small extent. It can also be said that when the laser field intensity exceeds $4 \times$ $10^{14} \, \text{W/cm}^2$, Case III, in which the ionization in the entire range within the duration of the laser pulse is considered, needs to be adopted for more reliable estimation of the final populations in the two levels. When the intensity exceeds $6 \times 10^{14} \, \text{W/cm}^2$, the depletion of neutral N_2 has to be incorporated to discuss the final populations.

V. CONCLUSION

By adopting the rovibronic model in which the electronic, vibrational, and rotational degrees of freedom of N_2^+ are included, we have investigated the dependence of the population transfer among the three low-lying electronic states, $X\,^2\Sigma_g^+$, $A\,^2\Pi_u$, and $B\,^2\Sigma_u^+$, induced by the postionization excitation in an ultrashort intense laser field. Based on the final population distribution among the vibrational states in the three electronic states and the population distribution among the rotational levels, we have revealed that the population inversion between the $X\,^2\Sigma_g^+(v=0)$ state and $B\,^2\Sigma_u^+(v=0)$ state can be realized in the specific rotational quantum ranges in the R- and P branches when ionization occurs around the central peak of the temporal shape of the laser field intensity. We have also simulated the dependence of the population transfer on the ionization timing by adopting the vibronic model with the parameter specifying the alignment angle of the N-N axis of N_2^+ and the laser polarization direction as well as the simplest two-level model, and we have found that the final population in the $B\,^2\Sigma_u^+$ of N_2^+ obtained by the rovibronic model with the alignment parameter as well as the final population in the upper level in the two-level system exhibit a temporally asymmetric pattern with respect to the central peak of the oscillating laser field intensity within the ultrashort laser pulse, which comes from nonadiabaticity due to rapid variation of the envelope function of the ultrashort intense laser pulse.

Using the two-level model based on the quasistationary Floquet theory, we have further shown that the ionization can be assumed to proceed only at $t = 0$ as long as the laser field intensity is less than $4 \times 10^{14} \, \text{W/cm}^2$ and that the ionizations induced in the entire range within the laser pulse duration should be calculated and integrated when the field intensity becomes larger.

The theoretical models developed in the study, in which the effect of the timing of the ionization of N_2 within an ultrashort intense laser pulse is incorporated in the postionization excitation processes in N_2^+, have a general applicability to postionization excitation processes of atomic and molecular ions created in an ultrashort intense laser field.

[1] Q. Luo, W. Liu, and S. Chin, Lasing action in air induced by ultra-fast laser filamentation, Appl. Phys. B **76**, 337 (2003).

[2] A. Dogariu, J. B. Michael, M. O. Scully, and R. B. Miles, High-gain backward lasing in air, Science **331**, 442 (2011).

[3] P. R. Hemmer, R. B. Miles, P. Polynkin, T. Siebert, A. V. Sokolov, P. Sprangle, and M. O. Scully, Standoff spectroscopy via remote generation of a backward-propagating laser beam, Proc. Natl. Acad. Sci. USA **108**, 3130 (2011).

[4] S. Mitryukovskiy, Y. Liu, P. Ding, A. Houard, and A. Mysyrowicz, Backward stimulated radiation from filaments in nitrogen gas and air pumped by circularly polarized 800 nm femtosecond laser pulses, Opt. Express **22**, 12750 (2014).

[5] G. Point, Y. Liu, Y. Brelet, S. Mitryukovskiy, P. Ding, A. Houard, and A. Mysyrowicz, Lasing of ambient air with microjoule pulse energy pumped by a multi-terawatt infrared femtosecond laser, Opt. Lett. **39**, 1725 (2014).

[6] V. Kocharovsky, S. Cameron, K. Lehmann, R. Lucht, R. Miles, Y. Rostovtsev, W. Warren, G. R. Welch, and M. O. Scully, Gain-swept superradiance applied to the stand-off detection of trace impurities in the atmosphere, Proc. Natl. Acad. Sci. USA **102**, 7806 (2005).

[7] J. Yao, B. Zeng, H. Xu, G. Li, W. Chu, J. Ni, H. Zhang, S. L. Chin, Y. Cheng, and Z. Xu, High-brightness switchable multiwavelength remote laser in air, Phys. Rev. A **84**, 051802(R) (2011).

[8] T.-J. Wang, J. Ju, J.-F. Daigle, S. Yuan, R. Li, and S. L. Chin, Self-seeded forward lasing action from a femtosecond Ti:sapphire laser filament in air, Laser Phys. Lett. **10**, 125401 (2013).

[9] H. Xu, E. Lötstedt, A. Iwasaki, and K. Yamanouchi, Sub-10-fs population inversion in N_2^+ in air lasing through multiple state coupling, Nat. Commun. **6**, 8347 (2015).

[10] J. Yao, S. Jiang, W. Chu, B. Zeng, C. Wu, R. Lu, Z. Li, H. Xie, G. Li, C. Yu, Z. Wang, H. Jiang, Q. Gong, and Y. Cheng, Population Redistribution Among Multiple Electronic States of Molecular Nitrogen Ions in Strong Laser Fields, Phys. Rev. Lett. **116**, 143007 (2016).

[11] H. Xu, E. Lötstedt, T. Ando, A. Iwasaki, and K. Yamanouchi, Alignment-dependent population inversion in N_2^+ in intense few-cycle laser fields, Phys. Rev. A **96**, 041401(R) (2017).

[12] Y. Liu, P. Ding, N. Ibrakovic, S. Bengtsson, S. Chen, R. Danylo, E. R. Simpson, E. W. Larsen, X. Zhang, Z. Fan, A. Houard, J. Mauritsson, A. L'Huillier, C. L. Arnold, S. Zhuang, V. Tikhonchuk, and A. Mysyrowicz, Unexpected Sensitivity of Nitrogen Ions Superradiant Emission on Pump Laser Wavelength and Duration, Phys. Rev. Lett. **119**, 203205 (2017).

[13] X. Zhong, Z. Miao, L. Zhang, Q. Liang, M. Lei, H. Jiang, Y. Liu, Q. Gong, and C. Wu, Vibrational and electronic excitation of ionized nitrogen molecules in intense laser fields, Phys. Rev. A **96**, 043422 (2017).

[14] L. Arissian, B. Kamer, A. Rastegari, D. M. Villeneuve, and J.-C. Diels, Transient gain from N_2^+ in light filaments, Phys. Rev. A **98**, 053438 (2018).

[15] A. Zhang, Q. Liang, M. Lei, L. Yuan, Y. Liu, Z. Fan, X. Zhang, S. Zhuang, C. Wu, Q. Gong, and H. Jiang, Coherent modulation of superradiance from nitrogen ions pumped with femtosecond pulses, Opt. Express **27**, 12638 (2019).

[16] G. Li, C. Jing, B. Zeng, H. Xie, J. Yao, W. Chu, J. Ni, H. Zhang, H. Xu, Y. Cheng, and Z. Xu, Signature of superradiance from a nitrogen-gas plasma channel produced by strong-field ionization, Phys. Rev. A **89**, 033833 (2014).

[17] Y. Liu, P. Ding, G. Lambert, A. Houard, V. Tikhonchuk, and A. Mysyrowicz, Recollision-Induced Superradiance of Ionized Nitrogen Molecules, Phys. Rev. Lett. **115**, 133203 (2015).

[18] X. Zhong, Z. Miao, L. Zhang, H. Jiang, Y. Liu, Q. Gong, and C. Wu, Optimizing the 391-nm lasing intensity from ionized nitrogen molecules in 800-nm femtosecond laser fields, Phys. Rev. A **97**, 033409 (2018).

[19] Y. Zhang, E. Lötstedt, and K. Yamanouchi, Population inversion in a strongly driven two-level system at far-off resonance, J. Phys. B **50**, 185603 (2017).

[20] I. Maruyama, T. Sako, and K. Yamanouchi, Time-dependent nuclear wavepacket dynamics of H_2^+ by quasi-stationary Floquet approach, J. Phys. B **37**, 3919 (2004).

[21] Y. Zhang, E. Lötstedt, and K. Yamanouchi, Mechanism of population inversion in laser-driven N_2^+, J. Phys. B **52**, 055401 (2019).

[22] T. Ando, E. Lötstedt, A. Iwasaki, H. Li, Y. Fu, S. Wang, H. Xu, and K. Yamanouchi, Rotational, Vibrational, and Electronic Modulations in N_2^+ Lasing at 391 nm: Evidence of Coherent $B^2\Sigma_u^+ - X^2\Sigma_g^+ - A^2\Pi_u$ Coupling, Phys. Rev. Lett. **123**, 203201 (2019).

[23] H. Li, E. Lötstedt, H. Li, Y. Zhou, N. Dong, L. Deng, P. Lu, T. Ando, A. Iwasaki, Y. Fu, S. Wang, J. Wu, K. Yamanouchi, and H. Xu, Giant Enhancement of Air Lasing by Complete Population Inversion in N_2^+, Phys. Rev. Lett. **125**, 053201 (2020).

[24] H. Zhang, C. Jing, J. Yao, G. Li, B. Zeng, W. Chu, J. Ni, X. Hongqiang, H. Xu, S. Leang Chin, K. Yamanouchi, H. Sun, and Z. Xu, Rotational Coherence Encoded in an "Air-Laser" Spectrum of Nitrogen Molecular Ions in an Intense Laser Field, Phys. Rev. X **3**, 041009 (2013).

[25] B. Zeng, W. Chu, G. Li, J. Yao, H. Zhang, J. Ni, C. Jing, H. Xie, and Y. Cheng, Real-time observation of dynamics in rotational molecular wave packets by use of air-laser spectroscopy, Phys. Rev. A **89**, 042508 (2014).

[26] M. Lei, C. Wu, A. Zhang, Q. Gong, and H. Jiang, Population inversion in the rotational levels of the superradiant N_2^+ pumped by femtosecond laser pulses, Opt. Express **25**, 4535 (2017).

[27] A. Azarm, P. Corkum, and P. Polynkin, Optical gain in rotationally excited nitrogen molecular ions, Phys. Rev. A **96**, 051401(R) (2017).

[28] Y. Zhang, E. Lötstedt, and K. Yamanouchi, Rotationally induced population inversion between the $B^2\Sigma_u^+$ and $X^2\Sigma_g^+$ states of N_2^+ exposed to an intense laser pulse, Phys. Rev. A **101**, 053412 (2020).

[29] Y. Zhang, E. Lötstedt, T. Ando, A. Iwasaki, H. Xu, and K. Yamanouchi, Rotational population transfer through the $A^2\Pi_u - X^2\Sigma_g^+ - B^2\Sigma_u^+$ coupling in N_2^+ lasing, Phys. Rev. A **104**, 023107 (2021).

[30] H. Li, M. Hou, H. Zang, Y. Fu, E. Lötstedt, T. Ando, A. Iwasaki, K. Yamanouchi, and H. Xu, Significant Enhancement of N_2^+ Lasing by Polarization-Modulated Ultrashort Laser Pulses, Phys. Rev. Lett. **122**, 013202 (2019).

[31] S.-F. Zhao, C. Jin, A.-T. Le, T. F. Jiang, and C. D. Lin, Determination of structure parameters in strong-field tunneling ionization theory of molecules, Phys. Rev. A **81**, 033423 (2010).

[32] Z. Li, Y.-H. Kuan, X. Mu, Z. Miao, C. Wu, and W.-T. Liao, Ramsey interferometry through coherent $A^2\Pi_u - X^2\Sigma_g^+ - B^2\Sigma_u^+$ coupling coupling and population transfer in N_2^+ air laser, Opt. Lett. **45**, 6587 (2020).

[33] Q. Zhang, H. Xie, G. Li, X. Wang, H. Lei, J. Zhao, Z. Chen, J. Yao, Y. Cheng, and Z. Zhao, Sub-cycle coherent control of ionic dynamics via transient ionization injection, Commun. Phys. **3**, 50 (2020).

[34] V. T. Tikhonchuk, Y. Liu, R. Danylo, A. Houard, and A. Mysyrowicz, Modeling of the processes of ionization and excitation of nitrogen molecules by short and intense laser pulses, Phys. Rev. A **104**, 063116 (2021).

[35] P. Linstrom and E. W. G. Mallard, *NIST Chemistry Web-Book*, NIST Standard Reference Database Number 69 (NIST, Gaithersburg, 2020), doi: 10.18434/T4D303.

[36] J. M. Brown and A. Carrington, *Rotational Spectroscopy of Diatomic Molecules*, *Cambridge Molecular Science* (Cambridge University Press, Cambridge, 2003).

[37] Y. R. Liu, Y. Wu, J. G. Wang, O. Vendrell, V. Kimberg, and S. B. Zhang, Electron-rotation coupling in diatomics under strong-field excitation, Phys. Rev. A **102**, 033114 (2020).

[38] X. M. Tong and C. D. Lin, Empirical formula for static field ionization rates of atoms and molecules by lasers in the barrier-suppression regime, J. Phys. B **38**, 2593 (2005).

[39] S. R. Langhoff, C. W. Bauschlicher, and H. Partridge, Theoretical study of the N_2^+ Meinel system, J. Chem. Phys. **87**, 4716 (1987).

[40] S. R. Langhoff and C. W. Bauschlicher, Jr., Theoretical study of the first and second negative systems of N_2^+, J. Chem. Phys. **88**, 329 (1988).

[41] S.-I. Chu and D. A. Telnov, Beyond the Floquet theorem: Generalized Floquet formalisms and quasienergy methods for atomic and molecular multiphoton processes in intense laser fields, Phys. Rep. **390**, 1 (2004).

[42] H. A. Leth, L. B. Madsen, and K. Mølmer, Monte Carlo Wave Packet Theory of Dissociative Double Ionization, Phys. Rev. Lett. **103**, 183601 (2009).

[43] M. Richter, M. Lytova, F. Morales, S. Haessler, O. Smirnova, M. Spanner, and M. Ivanov, Rotational quantum beat lasing without inversion, Optica **7**, 586 (2020).